Preprints (www.preprints.org) | NOT PEER-REVIEWED | Posted: 21 May 2018 doi:10.20944/preprints201805.0271.v1

Article

Spatio-Temporal Visualisation of Reflections from Building Integrated Photovoltaics

Roland Schregle [1]*, Christian Renken [2] and Stephen Wittkopf [1]

[1] Lucerne University of Applied Sciences and Arts, School of Engineering and Architecture, Technikumstrasse 21, CH-6048 Horw, Switzerland
[2] CR Energie GmbH, Z.I. l'Epine 7, CH-1868 Collombey, Switzerland
* Correspondence: roland.schregle@hslu.ch; Tel.: +41 41 349 3626

Abstract: With the increasing adoption of building integrated photovoltaics (BIPV), concerns arise about potential glare. While recommended criteria to assess glare exist, it is challenging to apply these in the spatial and temporal domains and communicate the complex data to planning authorities and clients. In this paper we present a new computational workflow using annual daylight simulation, material modelling using bi-directional scattering distribution functions (BSDFs) and image-based postprocessing to obtain 3-dimensional renderings of cumulative annual irradiance and glare duration on the built environment. The annual daylight simulation considers relevant sun positions in high temporal resolution (15-minute timesteps) and measured BSDFs to model different PV materials. The postprocessing includes a relative irradiance visualisation comparing the impact of a proposed PV proportional to a reference material. It also includes a new spatio-temporal workflow to assess the glare duration based on recommended thresholds. We demonstrate this workflow with a case study of a proposed PV roof for a church, assessing the glare potential of two different PV materials. Our visualisations indicate glare durations well below the thresholds with satinated PVs, and in noncritical zones outside observer positions with standard PVs. Thus the proposed PV roof does not cause any disturbing glare.

Keywords: Building integrated photovoltaics; annual daylight simulation; reflection; RADIANCE; photon mapping; BSDF; HDR; image processing; feature detection

1. Introduction

The integration of photovoltaics (PV) into building façades as building integrated photovoltaics (BIPV) holds opportunities in meeting the increasing demand for renewable energy. BIPV significantly improves the energy balance of buildings and their autonomy. The dramatic cost reduction in recent years along with a diversity in available designs have motivated the increasing use of BIPV. The appearance of BIPV corresponds to that of glass façades, as PV modules are typically laminated with glass. This has in turn influenced the development of urban architecture, with a shift from traditional construction materials such as plaster or fibre cement towards an increasing prevalence of glass façades in general, and BIPV in particular.

A negative side effect of this development are potentially disturbing reflections from specular façades, which pose a challenge for building and environmental authorities. Reflections are problematic because they may negatively impact the well-being of occupants in adjacent buildings as well as pedestrians. Consequently there is a demand for criteria to assess the impact of such reflections.

1.1. Current Assessment Criteria

The acceptance of BIPV by architects, authorities and communities requires a high degree of flexibility in design, and a form of governance that limits reflections or glare from façades. Currently there is infact a surprising dearth of specific legislation to regulate these potentially harmful effects. While some practical guidelines do mention explicit criteria, they are intended as *recommendations*

© 2018 by the author(s). Distributed under a Creative Commons CC BY license.

Preprints (www.preprints.org) | NOT PEER-REVIEWED | Posted: 21 May 2018 doi:10.20944/preprints201805.0271.v1

rather than standards for compliance. This tolerance can be largely attributed to the highly subjective nature with which individuals perceive reflection as glare.

A recent comprehensive literature review on the problem of reflections from building façades was published in [1], which proposes using glare impact categories as criteria for assessing the reflections. However, the criteria are entirely subjective, and not photometrically quantified. It does, on the other hand, propose radiometric limits to quantify the thermal impact of reflections.

In Switzerland, BIPV in façades and areas of the building envelope except the roof are subject to approval by building and environmental authorities. By contrast, roof-mounted PV must comply with article 18a of the federal spatial planning law (Bundesgesetz über die Raumplanung, RPG [2]), which requires that they be "adequately adapted". Furthermore, the RPG is implemented for PV installations according to article 32a of the federal spatial planning ordinance (Raumplanungsverordnung, RPV [3]), which simply states that PV installations are to be of low reflectance, in accordance with the state of the art.

An informal survey was conducted by the authors with building authorities in four Swiss Cantons (Bern, Basel, Neuenburg/Neuchâtel and Zürich) to determine whether specific requirements for glare protection from BIPV have been established locally. The survey revealed that none of the regional authorities currently enforce definite criteria for PV installations beyond those cited in the RPV, and in particular no specific parameters to identify potential glare from reflections.

The Swiss federal environmental agency (Bundesamt für Umwelt, BAFU) has prepared a draft proposal that regulates emissions from artificial lighting and reflections from building façades as well as PV installations, but does not specify actual limits for glare [4]. Infact, the current proposal recommends that, if in doubt, the decision on whether a particular reflection is tolerable or not should be based on subjective expert opinion during an on-site inspection.

The German federal/state association for pollution control (Bund/Länder-Arbeitsgemeinschaft für Immissionsschutz, LAI) has issued a report with guidelines to measure, assess, and reduce light emissions [5]. This document explicitly states recommendations, quantifies influencing factors and mentions specific parameters to assess critial emissions from artificial lighting and building façades. On the basis of the abovementioned publications, Swissolar has issued a guideline with specific criteria relevant to PV installations for practitioners [6].

The objective criteria we have adopted for our analysis are primarily based on the specific recommendations issued by Swissolar. These parameters, together with their thresholds, are summarised in Table A1 in the appendix. The most relevant of these criteria in assessing potential glare are primarily the reflection luminance, with the irradiance on a receiver due to reflection as complementary criterion.

Unfortunately, luminance is dependent on viewpoints facing the emitting building, and must be fixed for each simulation run, possibly requiring multiple iterations. Viewpoint placement requires a priori knowledge or anticipation of where glare is likely to occur; a tool cannot support the planner in this decision. The irradiance on the built environment, on the other hand, can be rendered in one image to concisely convey areas of potential glare as seen from the emitting building; such a visualisation can be readily grasped by nonexpert clients and municipal decision-makers. If potentially problematic glare zones are discovered, these can be further investigated from the corresponding viewpoint as luminance. We therefore propose an irradiance-based approach in our workflow as an initial step in assessing a planned PV installation.

Swissolar recommends an irradiance threshold of 30 W/m^2 for reflections based on a theoretical maximum direct normal irradiance of ca. 800–1000 W/m^2 at medium altitude (typically higher on an inclined PV panel) and a reflectance of ca. 3–4% [1]. However, an analysis of glint and glare from solar power plants conducted by Sandia National Laboratories [7] reports that a solar irradiance of

[1] Personal communication with Peter Toggweiler, Senior Technical Consultant for Basler & Hoffmann, Zürich, 27.03.2018.

Preprints (www.preprints.org) | NOT PEER-REVIEWED | Posted: 21 May 2018 doi:10.20944/preprints201805.0271.v1

only 1–10 W/m^2 at the eye can already lead to temporary blindness and afterimages. This analysis was based on retinal irradiance metrics collated from experimental data. Glint constitutes short-term glare that can be particularly hazardous to air and ground traffic, with recovery times for the aforesaid irradiance range lasting 0.8 to 12 seconds in experiments. Based on this evidence, we also include an alternative, more conservative irradiance threshold of 10 W/m^2 in our analysis.

1.2. PV Reflection Analysis

Reflections from PV are transient in time and space over the course of a year, and thus difficult to predict. A reliable annual prediction on the basis of computational simulation can therefore complement the practitioner's experience in selecting a candidate PV installation. Ideally, this analysis should be applied in the pre-project planning phase of a PV proposal to identify potentially disturbing reflections at an early stage. The results can then lead to adjustments to the project while still in the planning phase. In addition, authorities issuing building permits can base their decisions on the analysis. This avoids incurring additional expenses for subsequent adjustments in the course of the project, or additional consultancy for more elaborate reflection analyses.

In this paper we propose a simulation workflow to assess PV reflection, which we demonstrate with a case study of a PV retrofit sited in Lucerne, Switzerland. Our method calculates reflection from the PV and the resulting irradiance on the surrounding buildings. The irradiance is resolved spatially and temporally as a time-series of rendered high dynamic range (HDR) images, which we refer to as *irradiance maps*. The irradiance is then evaluated according to the recommended criteria in Table A1 to assess the maximum sustained glare duration per day (as worst case), and cumulative glare duration per year.

There are few documented instances of simulation tools to specifically assess PV reflection. One promising example is an interactive system developed at Fraunhofer FIT specifically to analyse glint and glare from PV at airports [8]. At the time of writing, this system only considered total specular reflection using an analytical BSDF model, ignoring the potentially significant diffuse component. Furthermore, the system does not consider the topography of the built environment (which is typically flat around airports), nor any of the abovementioned recommended thresholds in its assessment.

The sophisticated Solar Glare Hazard Analysis Tool (SGHAT) developed by Sandia National Laboratories [9] offers a convenient web-based interface using the Google Maps API. The user can select a region populated by PV superimposed on satellite imagery and adjust a multitude of parameters, such as PV tilt, orientation, elevation, and reflectance. The user must then select fixed observation points, for which the tool generates annual glare occurrence plots in three categories – including permanent eye damage – according to the retinal hazard metrics collated by Sandia Labs [7]. Like Fraunhofer's system, SGHAT is primarily aimed at air traffic and satisfies FAA requirements. Unfortunately the tool is now restricted to military, state, and federal government users only, and its support ended in 2017. The SGHAT software is currently being licensed by Sims Industries as part of their ForgeSolar PV glare analysis toolset [10], which incorporates many of the aforesaid features and is available to registered users.

Our PV reflection analysis workflow primarily builds on earlier work by Yang [11], which applied forward raytracing and simplified density estimation to locate reflections from a building façade on a 3D model of its surrounding built environment. This was implemented on a parametric design platform comprised of RHINO and GRASSHOPPER.

Our workflow also leverages forward raytracing and density estimation, but in the unified context of the RADIANCE lighting simulation software suite [12] and its photon mapping extension [13]. We improve on the previous work by using data-driven BSDF models of the measured PV samples for a more accurate prediction of both specular and diffuse reflection. Furthermore, we benefit from the higher quality specular-diffuse reflections obtained with the photon map's forward raytracing algorithm.

Preprints (www.preprints.org) | NOT PEER-REVIEWED | Posted: 21 May 2018 doi:10.20944/preprints201805.0271.v1

Figure 1. Aerial view of St. Michael's church with parish in foreground, looking northeast.

1.3. Case Study

The church St. Michael in Lucerne was built in 1967 by the architect Hanns A. Brütsch [14]. He is an award-winning reformer of modern ecclesiastical architecture in Switzerland. The design of St. Michael is an example of *beton brut* creating sharp-edged expressive building volumes with exposed concrete. The building encloses the patio with an entrance and gathering space while resembling a fortress from the street view. Figure 1 shows the church in its current state in the context of its surroundings.

There are several large roof spaces, which were up for energy retrofit in 2010. But being an icon of *beton brut*, the church is a heritage protected site and as such, retrofit projects must maintain the original materials, construction and appearance. Initial applications to mount PV modules to some parts of the old roof were hence rejected by the municipal heritage board.

Figure 2 shows the original site plan. The roof slopes annotated in handwriting indicate the roof sections identified for PV coverage. Two sections face west with a slope of 27%, while one section faces south with a slope of 35%. As such, the heritage board was concerned with disturbing reflections from the proposed roof sections. The proposed PV system installer visualised the zones potentially affected by reflections in Figure 3 but could not make a conclusive verdict on the potential for glare. For this and other reasons, the project was put on hold.

A new attempt was made recently, in which the retrofit concept proposed to completely replace three larger roof sections with integrated photovoltaics. The PV roof shall visually maintain the small grained texture of the old roof tiles, and the construction details along eaves and verges shall follow the old dimensions, yet replace timber and fibre cement with metal and glass. In addition, the glare issue should be investigated by computational simulation to make informed decisions about zones and duration of potential glare, taking into account the material properties of different PV frontglass surfaces.

Preprints (www.preprints.org) | NOT PEER-REVIEWED | Posted: 21 May 2018 doi:10.20944/preprints201805.0271.v1

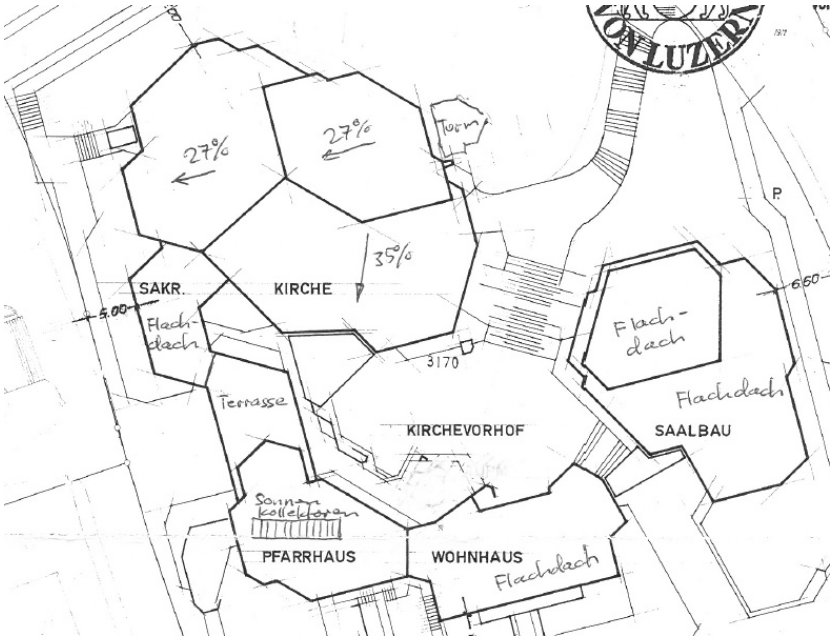

Figure 2. Original roof plan of St. Michael's church indicating slopes of each roof section.

2. Simulation Methodology

2.1. Motivation

The primary objective of our simulation is to provide a visual prediction of potential glare zones in the context of the built environment around a planned BIPV installation. As proposed in the introduction, this can be gleaned from a single representative irradiance map condensed from a large time-series of irradiance maps encompassing a half-year; the second half-year is identical due to analemmatic symmetry. Generally, a planner is not interested in assessing individual point-in-time renderings, but in the aggregate result over the course of a year; the visualisation should therefore convey this by reducing the 3-dimensional spatio-temporal data to a 2-dimensional image. As such, our workflow is entirely image based, and all processing operates on irradiance maps.

Using irradiance maps provides an initial qualitative analysis that fundamentally clarifies the presence or absence of potential glare as a first step in planning a PV installation. This saves the planner the burden of selecting observation points for a more comprehensive luminance analysis, e.g. in order to apply glare probability metrics. Such an analysis would then only be warranted for zones ("hotspots") in the irradiance maps indicating potential glare.

Falsecolouring the composite irradiance map with a colour scale provides a quantitative assessment to directly apply criteria such as cumulative and maximum glare duration in hours. At the same time, only the essential data is presented, thus the visualisations are also comprehensible to non-expert decision makers who may review the results during the building permit application process.

Because we are only interested in PV reflections, irradiance from other sources – notably the direct component from the sun – is not falsecoloured, but composited into the visualisation in greyscale to aid in orientation and identify affected buildings in the environment. Our workflow follows from this, and we render the direct and PV reflection irradiance maps separately, falsecolouring the latter before compositing both. More importantly, this also avoids false glare in panoramic views, since the sun paths are visible in the direct irradiance maps.

Each irradiance map in the time-series is rendered using RADIANCE in photon mapping mode. Because photon mapping traces rays from the light sources (suns) towards the receivers (built

Preprints (www.preprints.org) | NOT PEER-REVIEWED | Posted: 21 May 2018 doi:10.20944/preprints201805.0271.v1

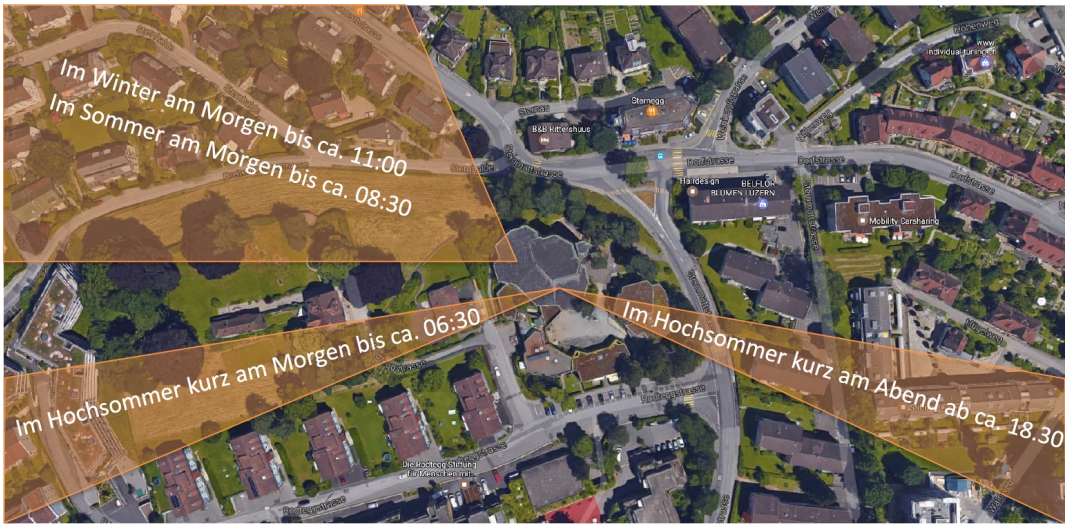

Figure 3. Reflection zones and timespans from roof of St. Michael's church predicted by PV system installer for initially proposed roof PV retrofit. Image courtesy of BE Netz AG.

environment), it excels at simulating specular-diffuse transfers, or *caustics*. Depending on its specularity, the PV surface material can effectively redirect daylight towards the built environment as caustics. Photons are deposited and stored on the surrounding diffuse surfaces, and may be reused for subsequent renderings. The RADIANCE photon map also supports time-series renderings by tagging each photon with its emitting light source (sun position) [13].

In addition to an efficient light transport algorithm, reliably predicting the irradiance reflected from PV also requires an accurate representation of the PV's reflecting behaviour. This is particularly important for standard PV modules with a glossy surface finish, which exhibit significant specular reflection. Consequently, we opt for a data-driven representation derived from measurements of actual candidate PV samples from our case study.

2.2. Workflow Overview

Our methodology consists of two workflows to visualise irradiance from PV reflection: a general workflow to assess cumulative annual irradiance, summarised in Figure 4, and a spatio-temporal workflow to assess glare duration according to recommended criteria, summarised in Figure 5. The latter builds on the former by using some of its output (photon map, simulation model, timesteps) and lies at the heart of our methodology.

Both workflows are managed in a UNIX Makefile which handles the multiple dependencies (corresponding to arrows in the flowcharts) and selectively runs individual components as targets. A separate simulation is run (technically an invocation of our Makefile) for each candidate PV material.

We have summarised the values chosen for the simulation parameters (shown on the left side of Figure 4) in Table B2 in the appendix. The workflow components are detailed in the following subsections.

2.3. General Workflow

The general workflow summarised in Figure 4 generates the timesteps, corresponding sky model and octree for the simulation. Furthermore, it simulates PV reflection by generating a photon map representing the incident flux on the built environment. These intermediate results are also used for the spatio-temporal workflow to apply criteria and evaluate glare duration.

The workflow visualises cumulative annual irradiance in absolute units (Wh/m^2) and relative to a reference material. The latter is primarily intended to compare the irradiance distribution of proposed

Preprints (www.preprints.org) | NOT PEER-REVIEWED | Posted: 21 May 2018 doi:10.20944/preprints201805.0271.v1

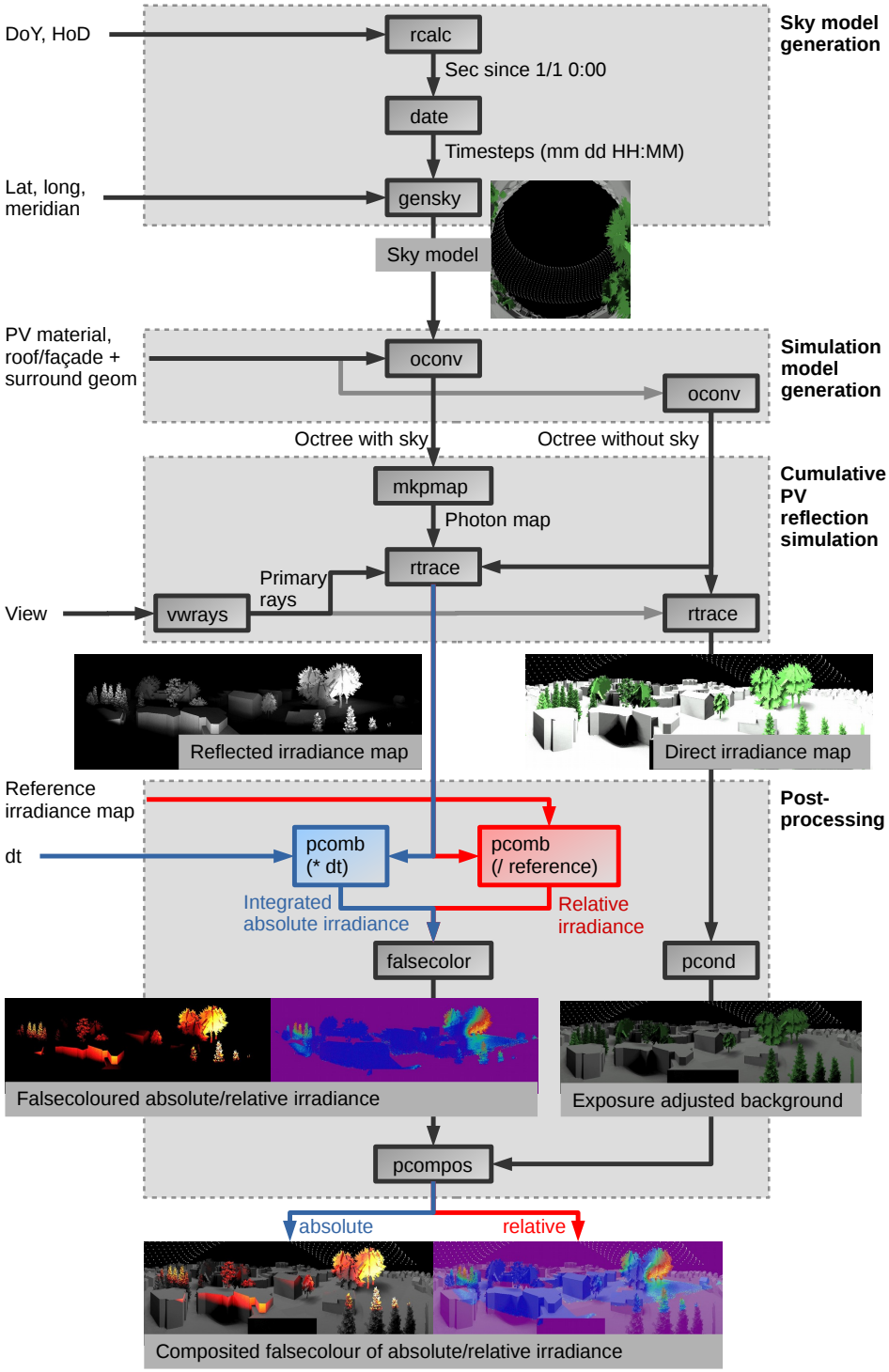

Figure 4. General PV reflection simulation workflow to assess cumulative annual irradiance.

and existing candidate materials. Both absolute and relative workflows share common components (shown in grey in Figure 4). Components specific to evaluating absolute irradiance are highlighted in blue, while those specific to relative irradiance are highlighted in red.

This simulation workflow is comprised of four stages: sky model generation, simulation model generation, cumulative PV reflection simulation, and postprocessing. These are detailed in the following subsections.

Preprints (www.preprints.org) | NOT PEER-REVIEWED | Posted: 21 May 2018 doi:10.20944/preprints201805.0271.v1

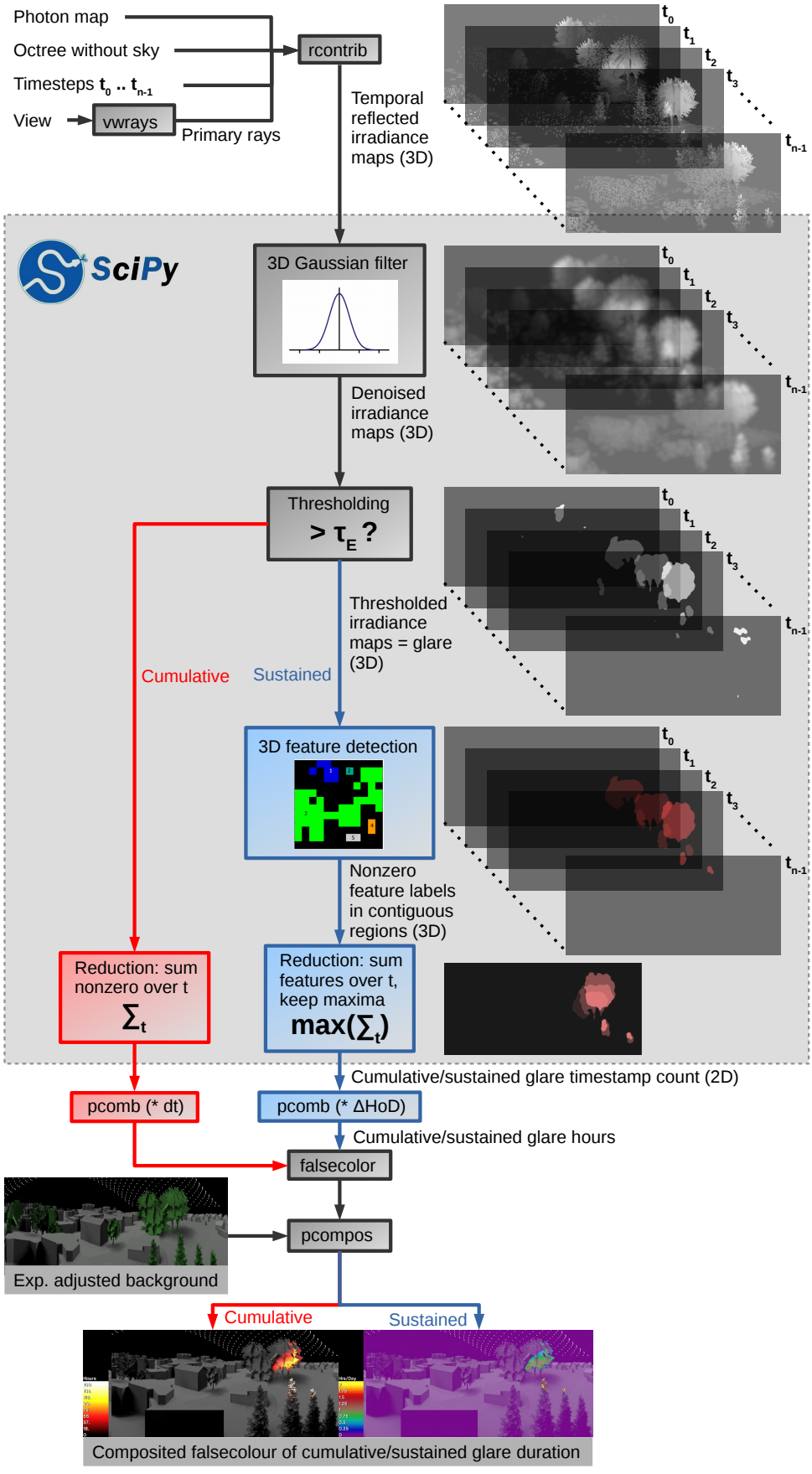

Figure 5. Spatio-temporal PV reflection simulation workflow to assess glare duration.

Preprints (www.preprints.org) | NOT PEER-REVIEWED | Posted: 21 May 2018 doi:10.20944/preprints201805.0271.v1

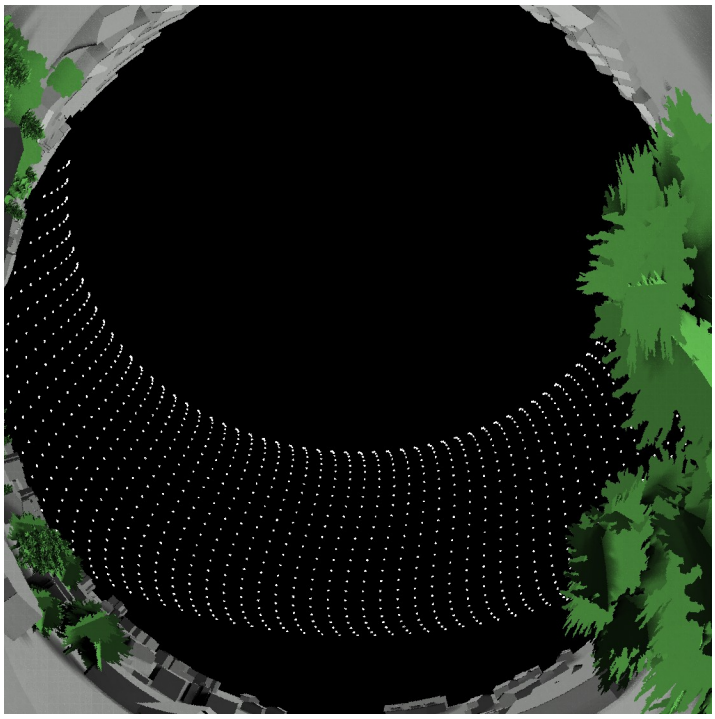

Figure 6. Fisheye view (hemispherical projection) of sunny sky model with 1280 timesteps as seen from roof, with south in the lower centre.

2.3.1. Sky Model Generation

In the initial simulation stage, we generate timesteps in fixed intervals, enumerated as day of year (DoY) since Jan. 1st, and local hour of day (HoD) for the current DoY. DoY and HoD are incremented by ΔDoY days and ΔHoD hours, respectively, with the latter being fractional. See Table B2 for timestep ranges and increments used in our case study.

Note that HoD increments can be coarse, as the sun paths progress very slowly on a daily basis. By contrast, sun paths change rapidly over the course of a day, and HoD is sampled densely. According the Nyquist Theorem, the latter should be sampled in at least 15-minute intervals to adequately resolve the maximum sustained glare duration threshold τ_t of 30 minutes in Table A1.

DoY and HoD are converted to absolute seconds with RADIANCE's *rcalc* utility and passed as seconds since the Epoch (Jan. 1st 1970 UTC) into the UNIX *date* utility, which generates the corresponding date and time in UTC. These timesteps are passed to RADIANCE's *gensky* tool to generate corresponding sky models. The timesteps are converted to local time for the specified timezone, latitude and longitude of the site under investigation.

To assess a worst case scenario, we generate a sunny sky consisting only of a distant light source representing the sun's position, without cloud cover. We accumulate a solar source for each timestep in a RADIANCE sky model file, with the exception of sun positions below the horizon (notably in the very early and late winter hours); these are ignored by *gensky*. With the DoY and HoD parameters in table Table B2 this results in 1280 timesteps / sun positions. These are shown in a hemispherical projection facing the zenith as seen at the site under investigation in Figure 6. Note that due to analemmatic symmetry, it suffices to simulate half a year, hence DoY is limited to 181. We compensate for the second half of the year by suitably weighting the accumulated irradiance during postprocessing in subsubsection 2.3.4.

Preprints (www.preprints.org) | NOT PEER-REVIEWED | Posted: 21 May 2018 doi:10.20944/preprints201805.0271.v1

2.3.2. Simulation Model Generation

The model for our simulation consists of the geometry of the site under investigation (roof or façade) as well as its immediate surroundings, at least within a radius of 100 m according to the recommended threshold τ_d in Table A1. In addition, PV material models PV are a critical ingredient; these should be reasonably accurate in modelling the scattering behaviour of the proposed candidate PV modules to obtain a realistic assessment of annual PV reflection. Both simulation components are detailed in the following subsections.

The geometric and material models are distilled along with the previously generated sky model into a RADIANCE scene octree with the *oconv* tool. Since our analysis primarily concerns the reflected component from the PV, we process this component separately. RADIANCE offers no immediate option to exclusively render this component, as such we generate an additional octree *without* sky model; in conjunction with the RADIANCE photon mapping extension, this can be used to only render the indirect irradiance from PV reflection. The octree with sky is used to render the direct component, which is used as background for our visualisation during postprocessing.

Geometric Model of Church and Surroundings

We obtained a digital terrain model of St. Michael's church and its built environment from the Geographic Information System of the Canton of Lucerne (GIS Kanton Luzern) [15]. This model was extracted from point cloud data obtained from LIDAR scans and is available to the public. Trees in the immediate environment of the church were identified from photographs and satellite images, and added with the RHINO 3D modelling software. In addition, minor corrections to the church roof geometry were made by hand based on the original blueprints. The entire geometry was then exported with RHINO to the RADIANCE format for the simulation. All surfaces were assigned lambertian materials with 25% reflectance.

Candidate PV Material Models

Samples of the proposed PV modules as well as the existing roof tiles were obtained from the manufacturers. The samples included a standard PV module exhibiting glossy reflection, and a satinated module with pronounced diffuse scattering more closely resembling the existing roof tile in appearance (see photographs in Figure 7). All three samples were analysed in terms of their scattering behaviour for the simulation. To this end, each sample was measured in our goniophotometer to obtain its BSDF (Bidirectional Scattering Distribution Function) [16], which was observed to be isotropic in all cases. Figure 8 shows polar plots of the measured PV BSDFs for two incident directions, with the existing tile BSDF superimposed as reference.

We modelled the candidate PV materials with the data-driven *bsdf* material primitive in RADIANCE, which reads the data from an XML file. The XML format describes a variable-resolution tensor tree representation of BSDF data [17], which is output by the *genbsdf* tool. The resulting data driven BSDF model has an angular resolution of up to 128 directions in the incident plane, and 128×128 in the exitant hemisphere. The resolution was adaptively reduced by thresholding the least significant 80% of data.

Figure 9 shows falsecolour RADIANCE luminance renderings of the data-driven BSDF models applied to the roof of our case study model. The renderings convey the appearance of the PV roof and the different scattering characteristics of the material models subject to the time of day. As expected from the BSDF plots, both the existing roof tile and satinated PV module exhibit predominantly diffuse scattering. On the other hand, the standard PV module exhibits pronounced specular reflection, particularly on summer mornings, conspicuously diverging in appearance from the original roof.

Preprints (www.preprints.org) | NOT PEER-REVIEWED | Posted: 21 May 2018 doi:10.20944/preprints201805.0271.v1

Figure 7. Photographs of samples used in our analysis: standard PV module **(a)**, satinated PV module **(b)**, and existing roof tile **(c)**.

2.3.3. Cumulative PV Reflection Simulation

The previously generated octrees (with and wihout sky) containing the simulation models are the basis for our PV reflection simulation. We precompute flux transport within the model by generating a photon map, then subsequently render it to evaluate the irradiance on the environment. Both steps are explained in the following sections.

Photon Map Generation

Our workflow uses the RADIANCE out-of-core photon mapping extension [13,18] developed specifically to efficiently simulate specular redirection with very large photon maps. Out-of-core techniques enable us to page photons on demand from disk, and maintain an active subset of these in-core in a custom cache. In addition, we use contribution photons to identify flux originating from individual sun positions corresponding to the timesteps to render the time-series irradiance maps in the spatio temporal workflow (see subsection 2.4).

The contribution photon map is generated with the *mkpmap* tool and written to a separate file for subsequent rendering. The photon map represents the precomputed light transport from the PV

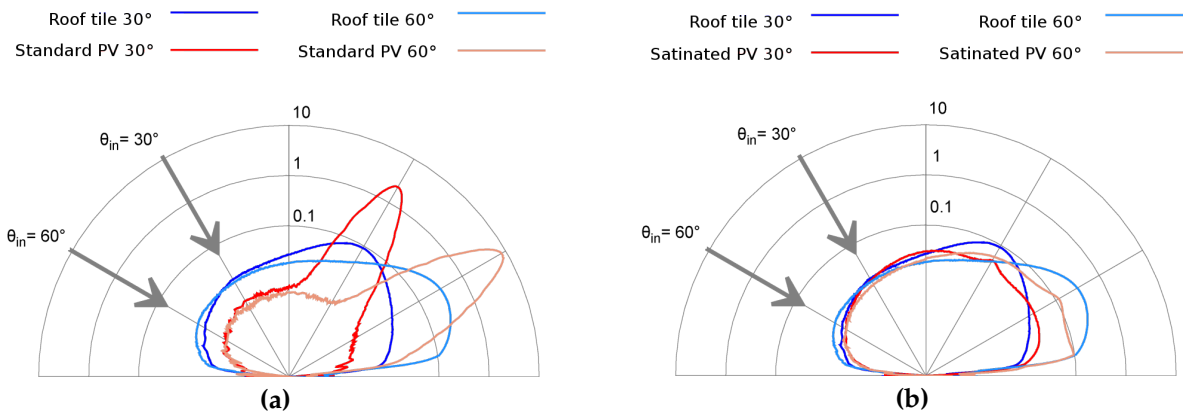

Figure 8. Polar BSDF plots of standard **(a)** and satinated **(b)** PV modules for incident angles of 30°(red) and 60°(brown). Corresponding BSDF plots of the existing roof tile (blue, cyan) are superimposed for comparison.

Preprints (www.preprints.org) | NOT PEER-REVIEWED | Posted: 21 May 2018 doi:10.20944/preprints201805.0271.v1

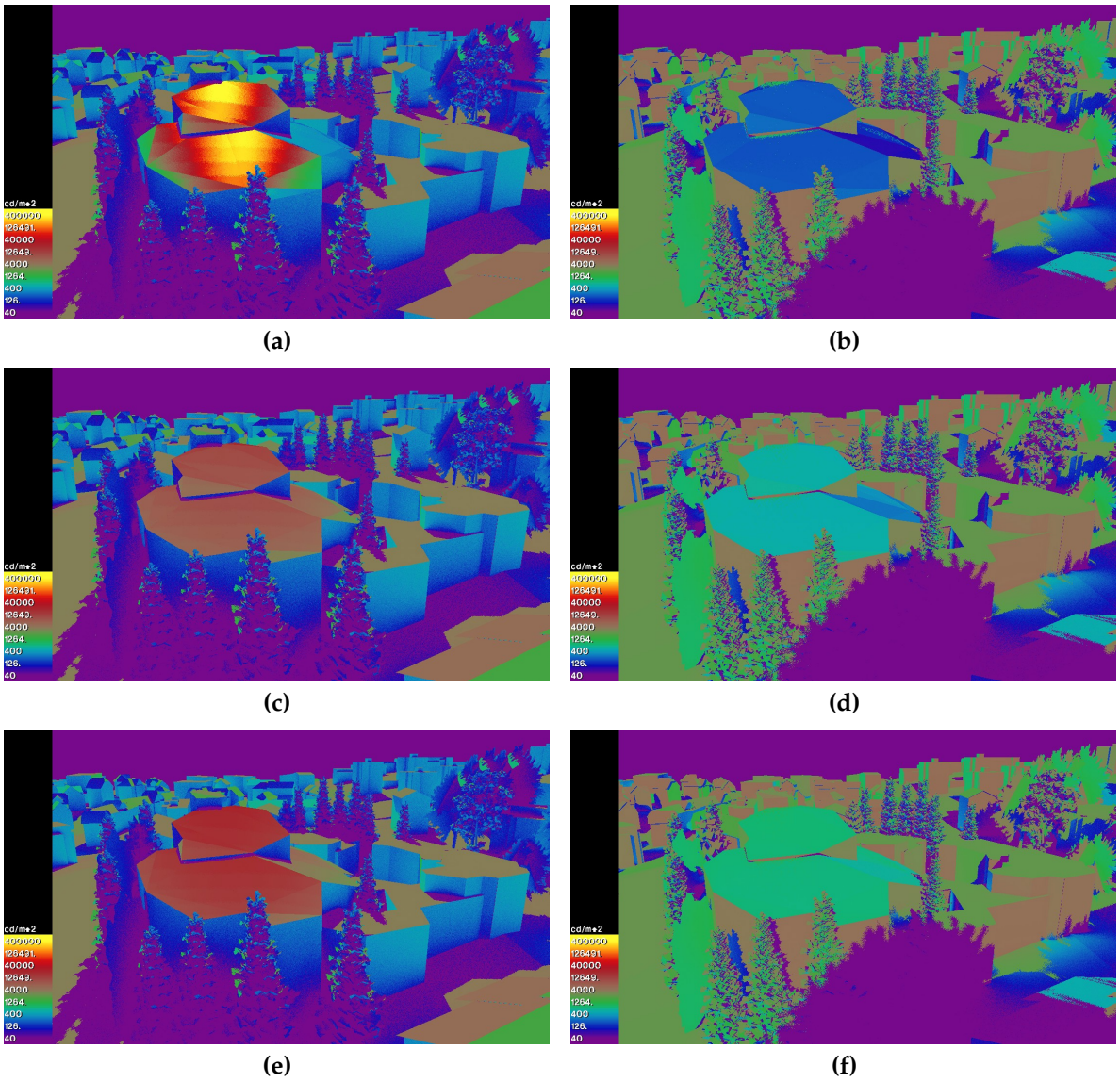

Figure 9. Falsecolour luminance renderings of our case study model looking east on June 11th at 8:30 AM **(a,c,e)** and 5:30 PM **(b,d,f)**. The roof material is modelled as a data-driven BSDF for the standard PV **(a,b)**, satinated PV **(c,d)**, and existing roof tile **(e,f)**. The distinc scattering behaviour of each BSDF is evident for the various times of day.

material onto the surrounding surfaces and can be reused for multiple renderings. *mkpmap* leverages the parallelism inherent in photon tracing since all photon paths are independent.

We employ a number of optimisations to reduce the photon count to the minimum required for our simulation, at the expense of increased photon distribution time (ca. 4 hours on an 8-core system with our case study). The photon transport is calculated for only a single reflection from the PV surfaces to the surroundings; we therefore force *mkpmap* to disregard secondary photon reflections by terminating the photons prematurely with the *-lr 1* option. Our rationale for this optimisation is that secondary reflections are negligible as long as the surroundings are diffuse.

In addition, we limit the photon paths to a cumulative length of 100 m with the *-ld* option, in accordance with the recommended criterion τ_d in Table A1; photons are again terminated beyond this distance, thus limiting their footprint to the region of interest. We can thus obtain acceptable results (in terms of noise) with a moderate number of photons.

Preprints (www.preprints.org) | NOT PEER-REVIEWED | Posted: 21 May 2018 doi:10.20944/preprints201805.0271.v1

Lastly, we use photon ports [19] to emit photons directly onto all PV surfaces (in our case, the roof), disregarding reflections from exterior walls or the surroundings. To this end, photons are displaced a small distance along the sun vector from the PV surfaces, and emitted towards them. Irregularly shaped polygons, as in the case of the roof of St. Michael's are handled via rejection sampling.

Rendering

We render PV reflection as a separate component using the previously generated photon map and RADIANCE octree without sky, thus omitting the direct component. The irradiance from the PV reflection onto the surroundings is evaluated via photon density estimates from the previously generated photon map with *rtrace*. This general raytracing tool in the RADIANCE suite supports parallel raytracing and can be used for rendering by passing in primary rays from a view via *vwrays*. The renderings are then output as RADIANCE HDR images. These are then postprocessed for visualisation of the reflected component as described in the following section.

The direct component is also rendered with *vwrays* / *rtrace* but using the octree with sky. The indirect (reflected) component is omitted by setting zero ambient bounces with the *-ab 0* option. The resulting direct irradiance map serves as background for the subsequent postprocessing.

Note that we render from two representative perspectives: a plan view as an overview for context, with the site under investigation in the centre, and a cylindrical projection as 360°panoramic view from the roof. The latter aids in identifying "hotspots" on adjacent buildings, as well as their corresponding directions. A fore clipping plane was used to prevent the church geometry from occluding the foreground.

2.3.4. Postprocessing

In the postprocessing phase we evaluate the rendered PV reflection irradiance maps. For the absolute annual irradiance, we derive Wh (Watt-hours) from the reflected irradiance on the built environment. For the relative annual irradiance, we derive a unitless ratio of reflected irradiance to that of the (previously rendered) reference case in order to compare the reflection distribution in the environment.

In both cases, the reflected irradiance map is falsecoloured and composited with the direct irradiance map. The latter is attenuated beforehand by *pcond* using the *-e* (exposure) option to provide a background for the visualisation to aid in orientation; it does not convey radiometric data.

The absolute and relative annual irradiance are derived separately as detailed in the following sections.

Absolute Annual Irradiance

To evaluate the absolute annual irradiance from PV reflection, we multiply the raw reflected irradiance data (consisting of cumulative irradiance proportional to the number of simulated timesteps) with an annual integration factor dt. We do this by scaling the HDR pixels in the reflected irradiance map by dt using the *pcomb* utility.

Given timesteps spanning half a year ($DoY \in [0, 181]$), the annual integration factor dt to obtain the cumulative irradiance in Watt-hours [Wh] can be approximated by:

$$dt \approx 2\Delta HoD \cdot \Delta DoY, \tag{1}$$

where the factor 2 compensates for the symmetric second half of the year. The accuracy of the integrated annual irradiance obviously depends on the increments ΔHoD and ΔDoY; smaller increments (and consequently more timesteps) will result in a finer grained simulation and more accurate results, at the expense of longer simulation and postprocessing.

Preprints (www.preprints.org) | NOT PEER-REVIEWED | Posted: 21 May 2018 doi:10.20944/preprints201805.0271.v1

Relative Annual Irradiance

To visualise the reflected irradiance distribution relative to that of a reference case we use *pcomb* to divide the reflected irradiance map pixels by those in the reference irradiance map (obtained from a previous simulation run with the reference material). We clamp the ratio to zero for pixels with zero irradiance (typically in peripheral or occluded areas, where no photons were deposited), thus avoiding divide by zero. The resulting image is unitless, with values above 1 indicating the PV reflection exceeds that of the reference, and values below 1 indicating the inverse.

2.4. Spatio-Temporal Workflow

The spatio-temporal workflow summarised in Figure 5 follows from the general workflow and reuses its generated simulation model, photon map, and timesteps. From these, it simultaneously renders temporal reflected irradiance maps for each timestep using the RADIANCE *rcontrib* tool. The photon map supports the association of flux contributions with individual solar sources (and corresponding timesteps) in order to evaluate the constituent irradiance at each timestep. As in the general workflow, the irradiance maps are rendered with an octree without sky to only visualise the reflected component; the direct irradiance map is reused here again as background for compositing the visualisation.

The goal of this workflow is to assess glare duration as primary criterion for identifying problematic glare zones, where glare is defined as reflected irradiance exceeding the threshold τ_E in Table A1. The output is a visualisation of the cumulative glare duration (as isolated events) over the course of a year, as well as the maximum *sustained* glare for any day of the year. The latter is derived from the maximum number of contiguous timesteps for which the irradiance exceeds the threshold without interruption. This implies temporal contiguity, which our workflow identifies using feature detection. As with the general workflow, both outputs share common components (shown in grey in figure Figure 5), and those specific to cumulative glare duration are highlighted in red, while those specific to sustained glare are highlighted in blue.

The postprocessing in this workflow is considerably more elaborate and mostly implemented with a Python script using the *ndimage* multi-dimensional image processing submodule as part of the SciPy scientific computing library [20]. The script processes a chronological time-series of irradiance maps as a 3-dimensional volume (2D matrices with an additional, temporal dimension).

The spatio-temporal postprocessing of the time-series irradiance maps consists of four main steps (five for sustained glare): filtering, thresholding, feature detection (for sustained glare), reduction, and visualisation. These are detailed in the following subsections.

2.4.1. Filtering

The 2D reflected irradiance maps rendered by *rcontrib* for each timestep are read from disk by our SciPy script and stacked in chronological order to form a spatio-temporal irradiance volume represented as a 3D matrix. Due to memory constraints and the high resolution of the irradiance maps, the timesteps will typically only encompass a single day, although the method would in principle work on the entire annual set of timesteps.

As the reflected irradiance maps are the result of Monte-Carlo raytracing with sparse photon distributions in dark areas, they exhibit considerable noise which can lead to unwanted temporal and spatial fluctuations after thresholding that break up potentially contiguous regions. We reduce the noise with a 3D Gaussian filter, thus improving temporal continuity and stabilising the subsequent thresholding. While this leads to a loss in detail, it instead emphasises large patches of glare, which is infact desirable for our purposes.

Preprints (www.preprints.org) | NOT PEER-REVIEWED | Posted: 21 May 2018 doi:10.20944/preprints201805.0271.v1

2.4.2. Thresholding

As the main criterion for identifying glare, we compare the filtered pixel in the irradiance volume against the recommended threshold τ_E in Table A1. This results in a binary values for each pixel indicating whether its corresponding irradiance is below or above the threshold; a nonzero value thus indicates the presence of glare according to the τ_E. Note that, although the pixels assume integer values, the ndimage library still treats the data as floating point, at the expense of increased memory consumption.

2.4.3. Feature Detection (Sustained Glare)

When assessing sustained glare, our workflow must identify neighbouring, i.e. contiguous, instances of glare along the spatial and temporal axes. This entails isolating regions of consecutive nonzero pixels (categorised as glare in the previous step) via feature detection. A method typically used in computer vision, feature detection attaches nonzero labels to neighbouring pixels. By applying this in three dimensions, we also account for temporal contiguity. The output is a new volume with nonzero integer labels in pixels categorised as glare over multiple consecutive timesteps. Each feature corresponds to a separate glare event and has a unique label.

2.4.4. Reduction

In this step, the 3D thresholded irradiance volume is reduced to a single 2D image for visualisation. For the cumulative glare duration, this entails simply summing the thresholded binary pixel values over the temporal axis.

For sustained glare, however, this entails summing (i.e. counting) all instances of pixels with nonzero labels along the temporal axis. We disregard the pixels' actual values, since these are unique for each contiguous region identified by the feature detection. In addition, disjunct features may overlap in time, e.g. if a pixel experiences several glare events in the course of a day from multiple PV surfaces. To account for this, we accumulate only the maximum number of nonzero pixels from all features, since a planner isprimarily interested in assessing the longest glare duration as worst-case scenario.

The output of both reductions is a 2D matrix containing an integer count of the number of timesteps corresponding to the cumulative or sustained glare duration. This is weighted accordingly in the final step of our workflow. In preparation for this, the matrices are written back to disk as RADIANCE HDR images, by our SciPy script, at which point it terminates.

As mentioned above, our workflow currently processes daily irradiance maps, consequently the resulting HDR images must be accumulated for the entire simulation run; this entails another level of reduction (accumulating maxima in the case of sustained glare) in a separate Python script, which is not shown in Figure 5.

2.4.5. Visualisation

The final step of our spatio-temporal workflow entails scaling the glare duration timestep count in the reduced HDR images, falsecolouring them, and compositing them with an attenuated background image of the direct irradiance as in the general workflow.

As in subsubsection 2.3.4, we scale the HDR images containing cumulative annual timestep counts with the annual integration factor dt (Equation 1) with RADIANCE's *pcomb* tool, resulting in cumulative annual glare duration in hours.

For sustained glare, however, we simply scale the HDR images with the hourly timestep increment, ΔHoD, to arrive at the corresponding maximum glare duration for any day of the year, in hours.

Preprints (www.preprints.org) | NOT PEER-REVIEWED | Posted: 21 May 2018 doi:10.20944/preprints201805.0271.v1

3. Results

3.1. Annual Reflected Irradiance

Plan views of the absolute cumulative annual irradiance reflected from the candidate PV and existing roof tile from our case study are shown in Figure 10. The church simulated roof material is located in the centre. Note the irradiance scale (Watt-hours) is logarithmic, and only applies to the falsecoloured reflected component. The direct component is composited as background for orientation to identify potentially affected buildings in the environment.

The reflection distribution relative to the existing roof tile is shown in Figure 11. The reflected component is again falsecoloured, this time on a linear scale as ratio of the annual reflected irradiance from the candidate PV divided by the annual reflected irradiance from the existing roof tile. The red/yellow regions (ratio > 1) indicate directions in which the PV reflects more intensely than the roof tile, while the blue regions (ratio < 1) indicate subdued PV reflection compared to the roof tile. Regions with zero reflection (due to occlusion or because they lie outside the zone of influence) are coloured magenta.

Figure 12 shows both the cumulative annual irradiance and relative reflection distribution as cylindrical panorama view from the church roof. The view faces south in the centre, while the left and right edges wrap around and face north. The sun paths comprising the sky model for the simulated half-year are clearly visible above the horizon. Part of the parish adjacent to the church can be seen in the foreground, while the church itself is clipped by the fore clipping plane so as not to occlude the view.

3.2. Glare Duration

Figure 13 shows panoramic views of the cumulative annual glare duration generated by our spatio-temporal workflow using irradiance thresholds of 30 W/m^2 and 10 W/m^2 as recommended by Swissolar, and Sandia Labs, respectively.

Figure 14 shows the maximum sustained glare duration for any day of the year, i.e. per-pixel glare duration maxima for all simulated days. Again, this is shown as panoramic views with irradiance thresholds of 30 W/m^2 and 10 W/m^2 as recommended by Swissolar, and Sandia Labs, respectively.

4. Discussion

4.1. Annual Irradiance

It is already evident from Figure 8 and Figure 9 that the candidate PV module BSDFs exhibit divergent scattering behaviour; while the standard PV is characterised by significant glossy reflection, the satinated PV is noticeably diffuse, and therefore resembles the scattering behaviour of the original roof tile.

This behaviour is corroborated in the renderings in section 3, particularly in the relative annual irradiance visualisations in Figure 11 and Figure 12(c,d); it is obvious from these results that the standard PV exhibits a pronounced heterogeneous reflection distribution, notably with a hotspot towards the west, while the satinated PV exhibits homogeneous reflection, on par with the existing roof tile used as reference.

While the bespoke hotspot in the west is evident in all renderings, it varies in intensity depending on the roof material. For the standard PV, the absolute cumulative annual irradiance shown in Figure 12(a,b) peaks in this zone at ca. 3000 Wh/m^2, but only at ca. 1000 Wh/m^2 for the satinated PV. We note that this hotspot coincides with a group trees shielding a 2-storey chalet behind them, as can be observed left of the plan views in Figure 10 and Figure 11.

This hotspot dominates in the early mornings in June, when the trees bear foliage. This is confirmed by the rendered luminance maps for June 11th at 8:30 AM in Figure 9(a,c,e), looking east

Preprints (www.preprints.org) | NOT PEER-REVIEWED | Posted: 21 May 2018 doi:10.20944/preprints201805.0271.v1

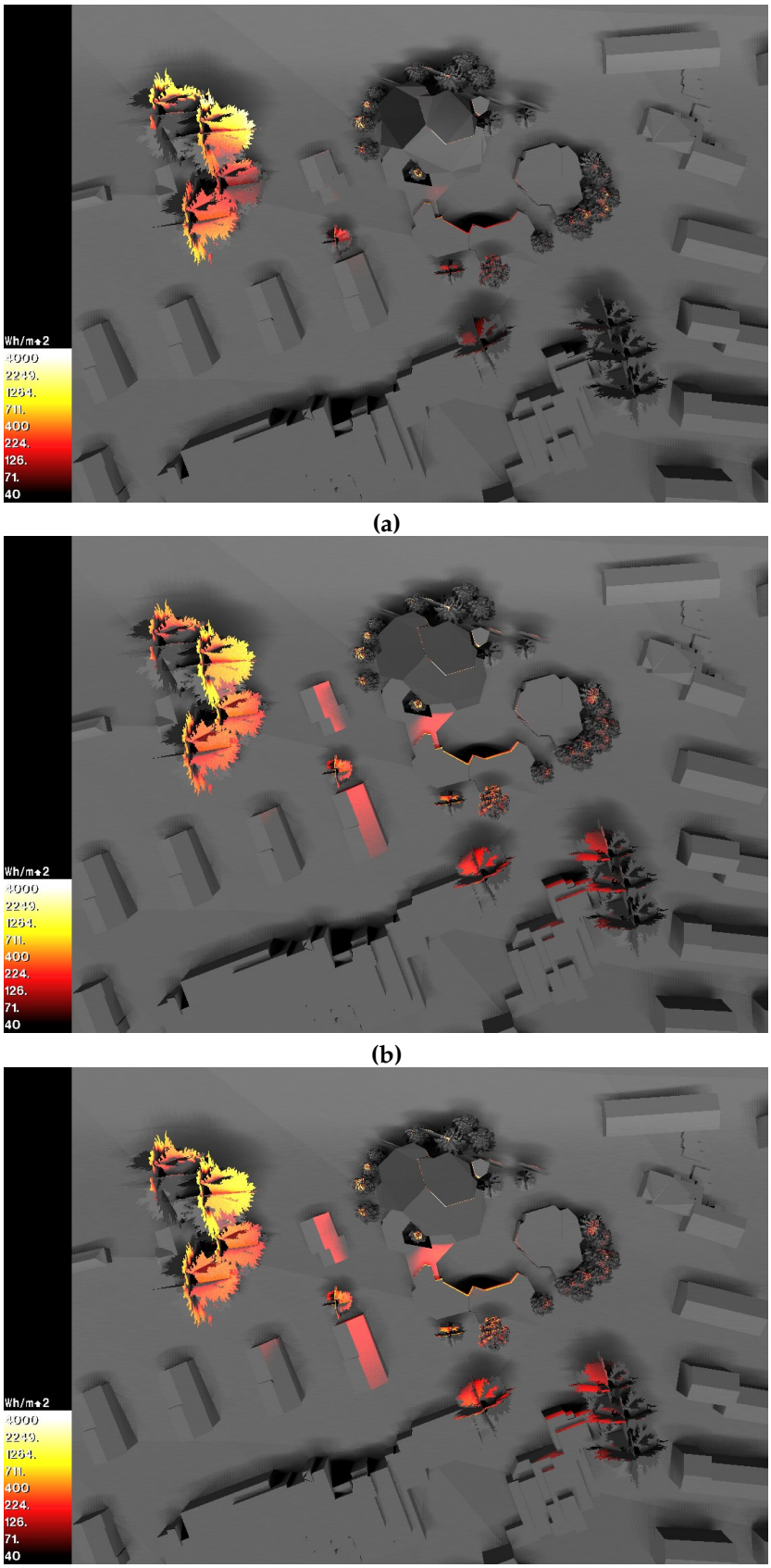

Figure 10. Plan views of absolute cumulative annual irradiance in Wh/m^2 from standard PV **(a)**, satinated PV **(b)** and existing roof tile **(c)**.

Preprints (www.preprints.org) | NOT PEER-REVIEWED | Posted: 21 May 2018 doi:10.20944/preprints201805.0271.v1

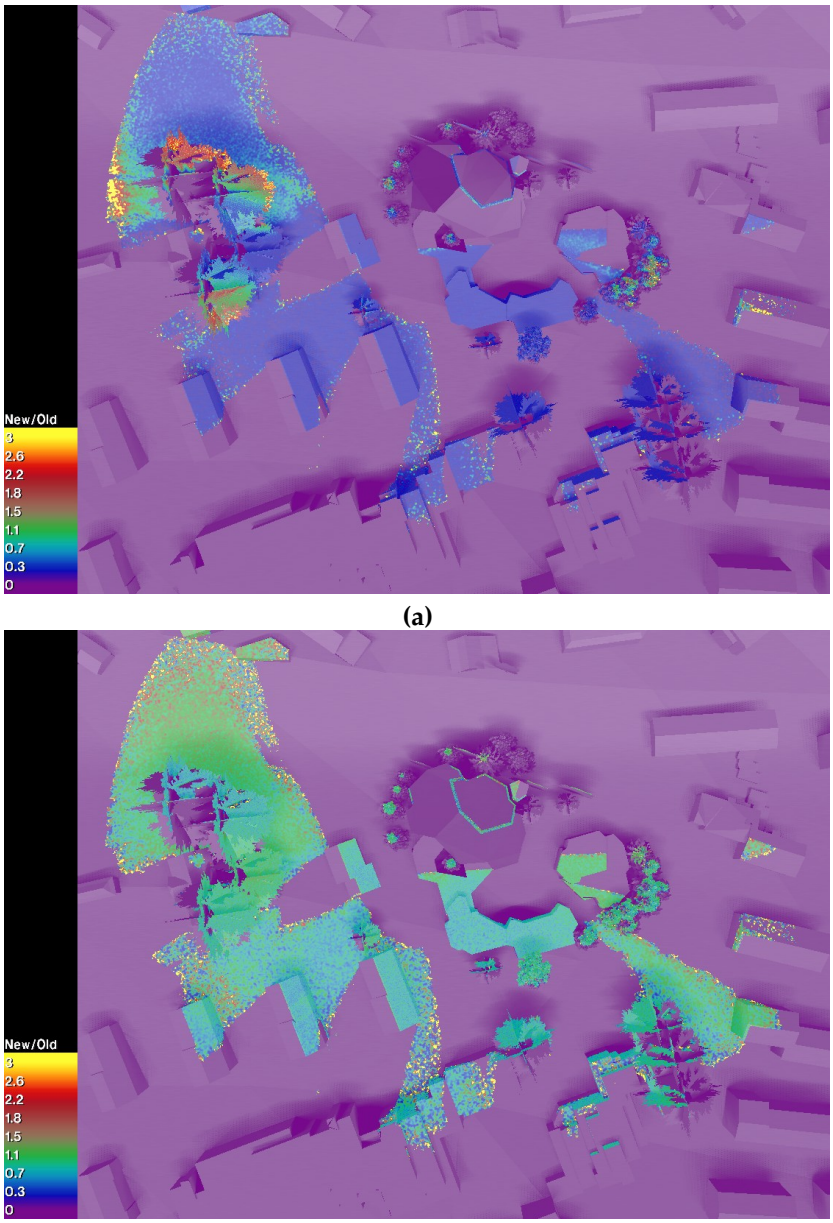

Figure 11. Plan views of relative irradiance distribution from standard **(a)** and satinated **(b)** PV compared to the existing roof tile.

from the approximate position of the hotpot. We note that the luminance from the standard PV module far exceeds the recommended threshold τ_L of 50 kcd/m^2 in Table A1, correlating with the potential for glare indicated by the irradiance map.

The results of our method agree well with the predictions made by the PV system installer for the first PV roof retrofit proposal from our case study. This is evident by superimposing the initial roof reflection plan from Figure 3 with a simulated plan view from Figure 10 obtained with our method. The resulting composite, shown in Figure 15, confirms the initial prediction in terms of the location and approximate timespan of the hotspots.

The mentioned hotspot on the group of trees in the west, predicted on summer mornings before ca. 8:30 AM, matches well. Note that while this initially predicted reflection zone extends towards the northwest, there are no buildings in this direction within the maximum distance τ_d of 100 m

Preprints (www.preprints.org) | NOT PEER-REVIEWED | Posted: 21 May 2018 doi:10.20944/preprints201805.0271.v1

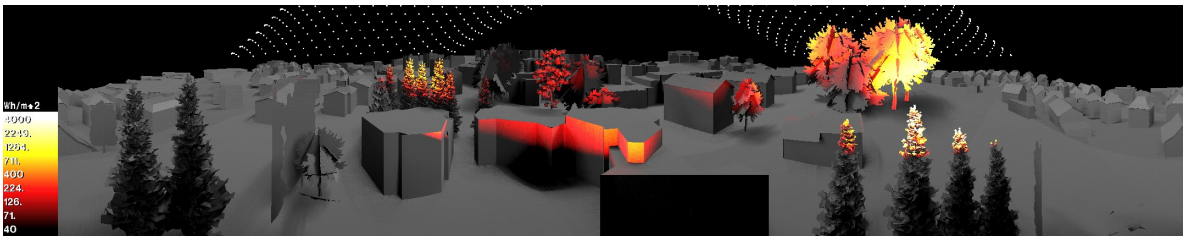

(a)

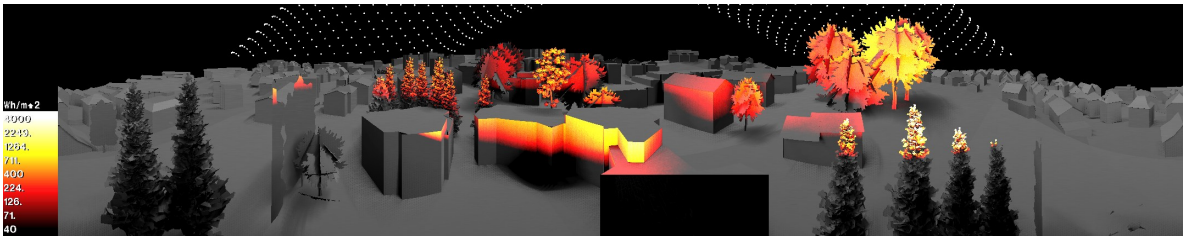

(b)

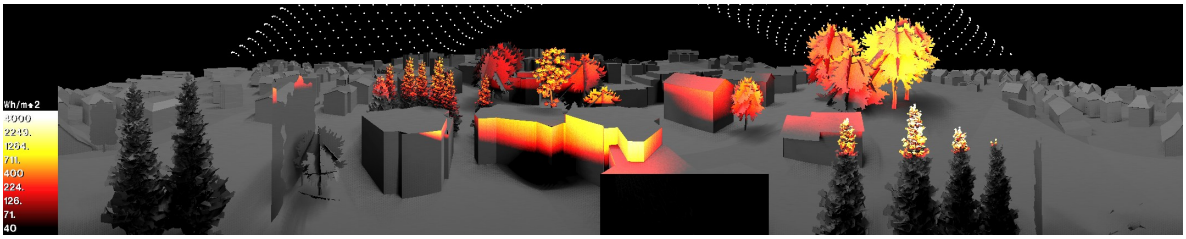

(c)

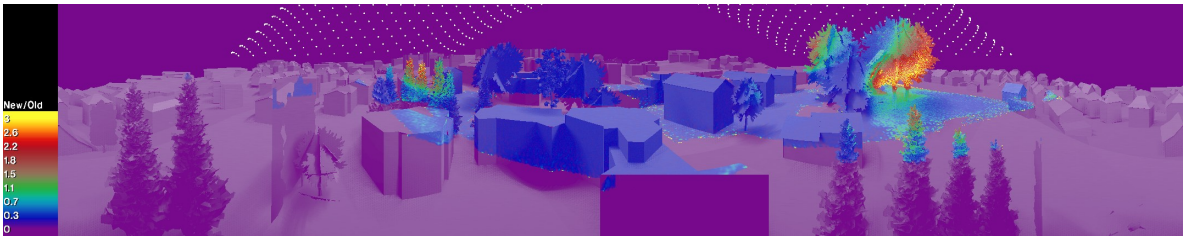

(d)

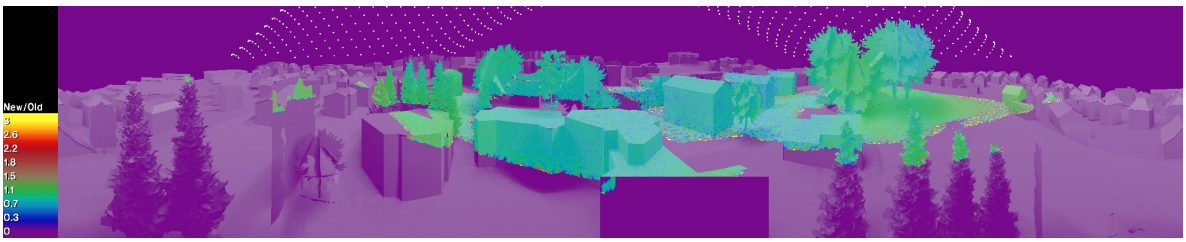

(e)

Figure 12. Panoramic views of annual irradiance from standard PV **(a, d)**, satinated PV **(b, e)** and existing roof tile **(c)**, with centre facing south. Figures **(a–c)** are in absolute units, while figures **(d–e)** are relative to the existing roof tile.

Preprints (www.preprints.org) | NOT PEER-REVIEWED | Posted: 21 May 2018 doi:10.20944/preprints201805.0271.v1

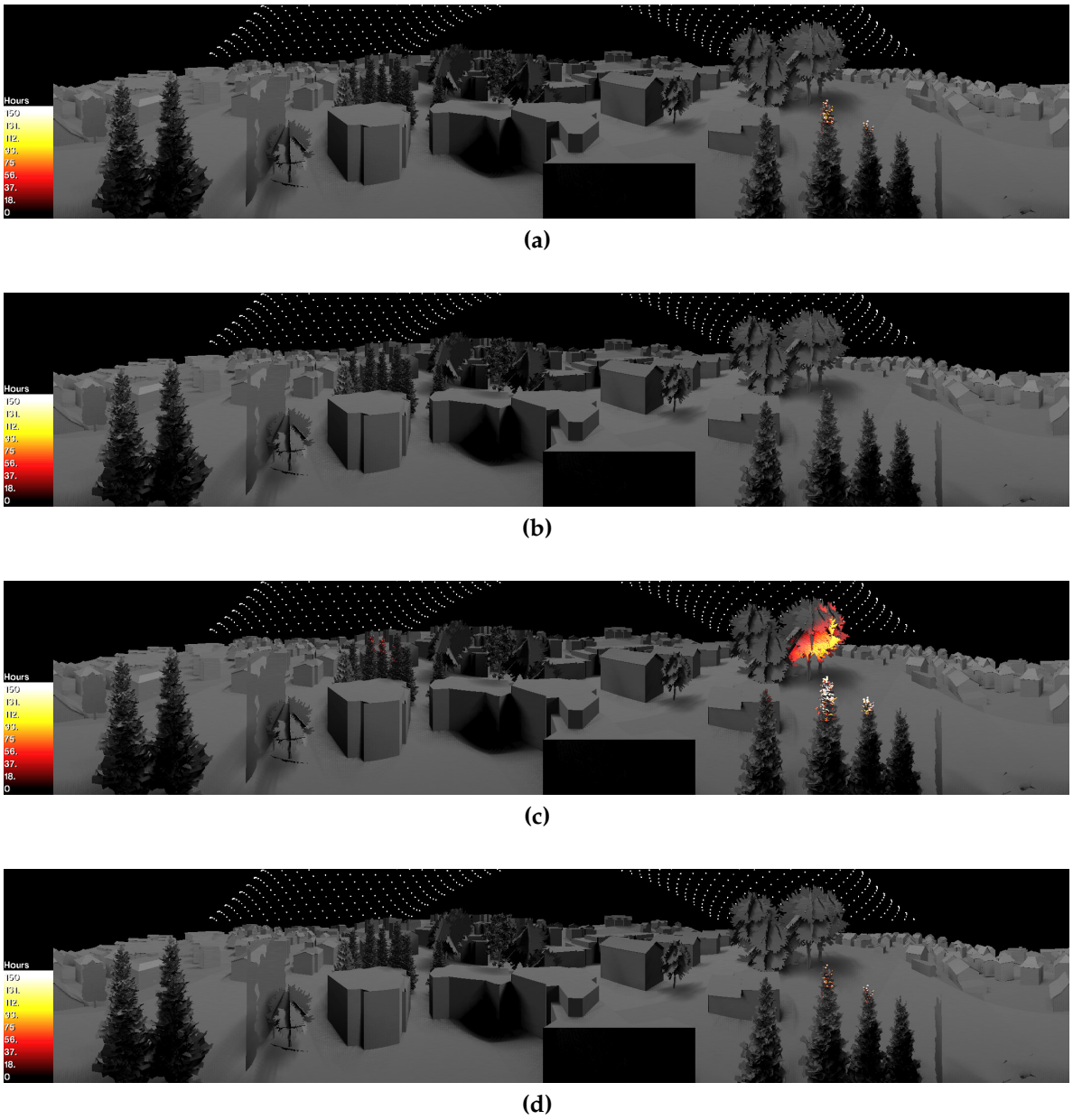

Figure 13. Panoramic views of cumulative annual glare duration in hours for standard **(a,c)** and satinated **(b,d)** PV modules. Glare is identified according to irradiance thresholds $\tau_E = 30\ \mathrm{W/m^2}$ as recommended by Swissolar **(a,b)**, and $\tau_E = 10\ \mathrm{W/m^2}$ as suggested by Sandia Labs **(c,d)**.

considered in our simulation. A secondary hotspot on the edge of the trees in the west-southwest on midsummer mornings before ca. 6:30 AM also matches. Lastly, minor hotspots on the treetops immediately adjoining the complex in the east-southeast on midsummer evenings after ca. 6:30 PM also correspond well.

4.2. Application of Recommended Critera, Glare Duration

To assess whether the noted hotspot is indeed problematic, we apply the irradiance thresholds τ_E in Table A1 to identify glare. With an irradiance threshold $\tau_E = 30\ \mathrm{W/m^2}$ as recommended by Swissolar, there is no annual glare whatsoever from either candidate PV, as shown in Figure 13 and Figure 14. In stark contrast, applying Sandia Labs' more conservative threshold $\tau_E = 10\ \mathrm{W/m^2}$ indicates significant

Preprints (www.preprints.org) | NOT PEER-REVIEWED | Posted: 21 May 2018 doi:10.20944/preprints201805.0271.v1

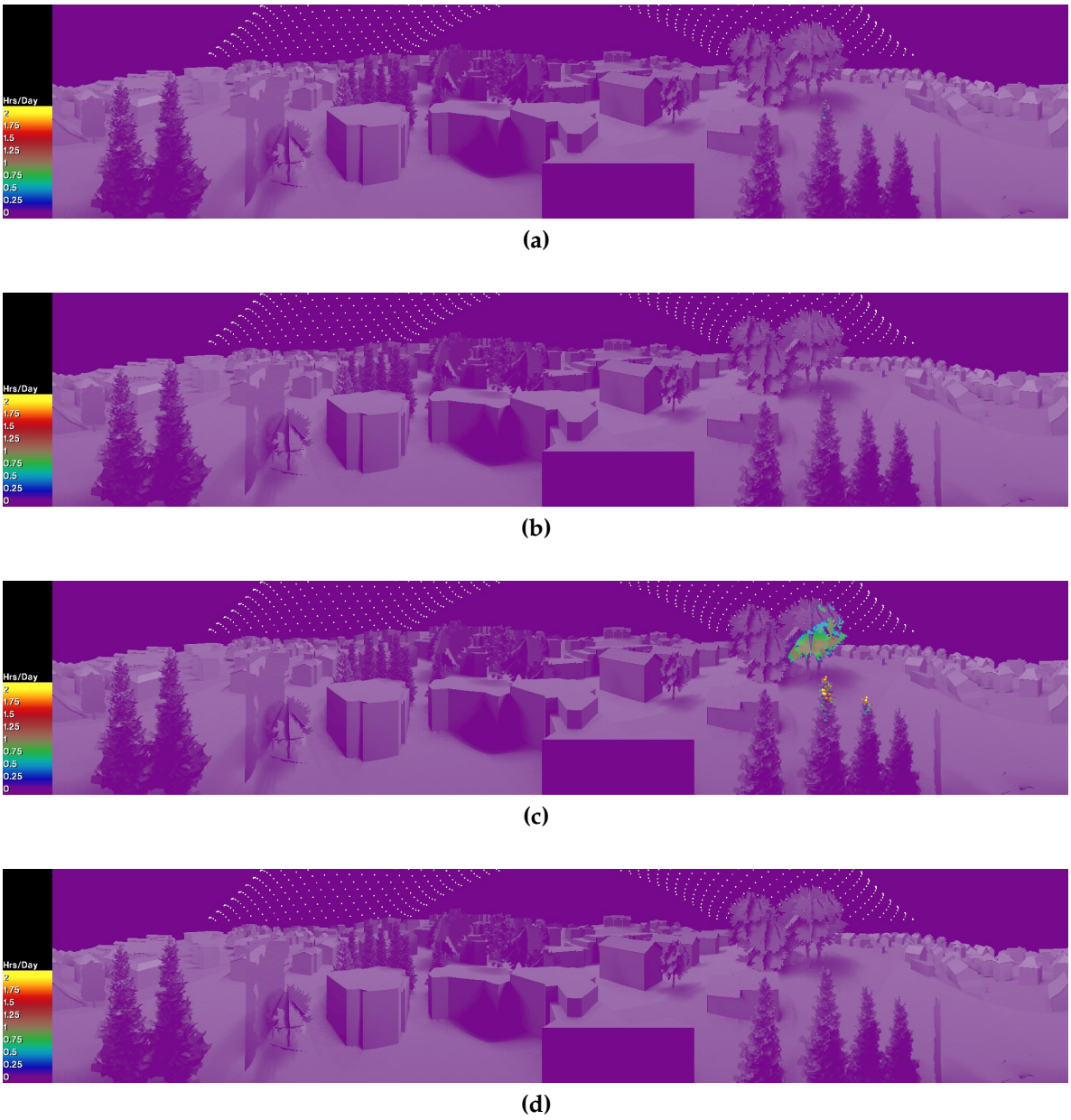

Figure 14. Panoramic views of maximum sustained glare duration in hours for any day of the year incurred by reflections from standard **(a,c)** and satinated **(b,d)** PV modules. Glare is identified according to irradiance thresholds $\tau_E = 30W/m^2$ as recommended by Swissolar **(a,b)**, and $\tau_E = 10W/m^2$ as suggested by Sandia Labs **(c,d)**.

annual glare durations of up to 100 hours in the bespoke group of trees with the standard PV module. This is twice the maximum annual duration τ_T of 50 hours recommended in Table A1.

As Figure 14 reveals for the same τ_E, this region experiences a maximum sustained glare duration of up to 1 hour; again, twice the maximum glare duration τ_t of 30 minutes for any day of the year as recommended in Table A1. These glare incidents would be considered problematic were they to lie on adjacent buildings, and would warrant a luminance-based assessment from the corresponding observation point. In the context of this case study, however, we assume vegetation is impervious to glare, and will not take any recourse.

We therefore consider both candidate PV materials to be viable for the retrofit and not critical in terms of glare. Subject to the constraints of the heritage protection board, the decision will likely be

Preprints (www.preprints.org) | NOT PEER-REVIEWED | Posted: 21 May 2018 doi:10.20944/preprints201805.0271.v1

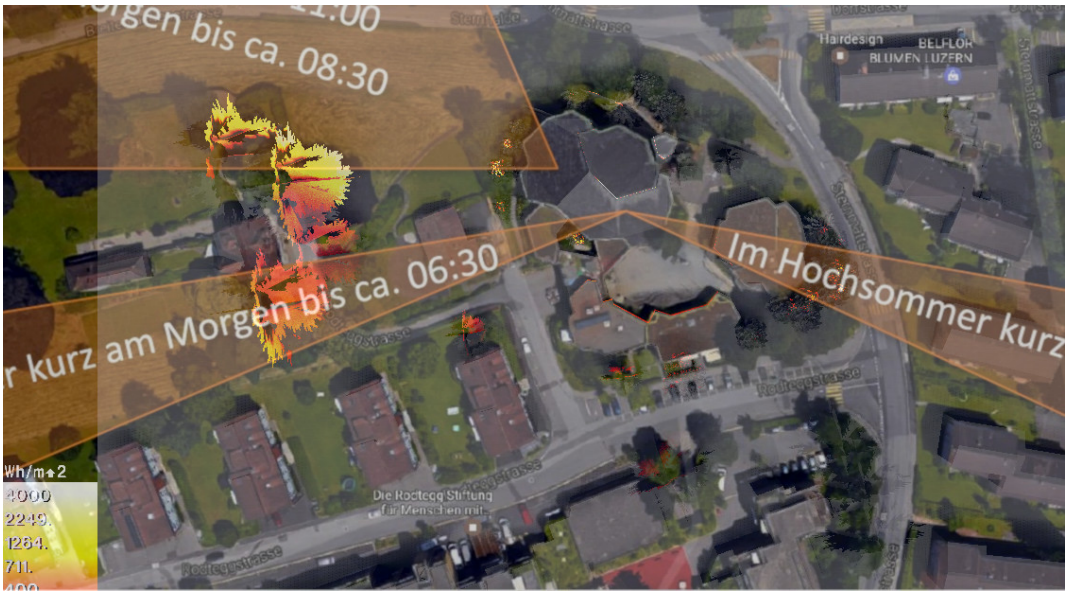

Figure 15. Reflection zones initially predicted by PV system installer (Figure 3) superimposed with plan view of simulated annual reflected irradiance obtained with our method (Figure 10).

based on which candidate better preserves the existing appearance of the roof, with the satinated PV clearly being the favourable choice.

5. Conclusion and Future Work

We have presented a novel image-based methodology for assessing glare from PV reflections and presenting the results in a visualisation suitable for practitioners, municipal planning authorities and clients of PV installations. Our methodology consists of a general workflow to assess cumulative annual irradiance from PV reflection, both in absolute terms and relative to a reference material in order to compare different candidate PV surface materials. In addition, we presented a novel spatio-temporal workflow to assess the cumulative annual glare duration, and the maximum sustained glare duration for any day of the year, according to few recommended criteria and thresholds currently available.

We have demonstrated our workflows with a representative case study of a PV roof retrofit for a church under heritage protection. Our PV reflection simulation used data-driven material models of measured BSDFs from a standard and satinated candidate PV module. In addition, we used photon mapping to efficiently precompute only the reflected component from the PV roof, which we visualised in falsecolour. We identified glare by applying two irradiance thresholds recommended by Swissolar and Sandia Labs. With the latter, more conservative threshold, we demonstrated the ability of our method to detect glare in instances when the reflected significantly irradiance exceeds the threshold for extended periods.

Based on the results and the recommended limits for glare duration (both cumulative annual and maximum sustained for any day of the year), we conclude that the satinated PV module causes no potential glare at all, while the standard PV module may give rise to considerable glare, but in irrelevant regions populated by vegetation. By comparing the results of our workflow with predictions made by the PV system installer in an earlier proposal of a PV roof retrofit for our case study, we have confirmed that our method indeed complements and supports the expertise of a PV planner.

We emphasise that applying the recommended criteria in our workflow does not constitute their validation. Whether the predicted glare is actually perceived as disturbing is, as the criteria themselves, highly subjective. We note, however, that the irradiance threshold recommended by Swissolar is based on a theoretical maximum, whereas Sandia Labs' is based on experimental data. If in doubt, the latter would be preferable to rule out any possibility of glare.

Preprints (www.preprints.org) | NOT PEER-REVIEWED | Posted: 21 May 2018 doi:10.20944/preprints201805.0271.v1

Our methodology is still a proof of concept both in terms of technological realisation and visualisation of the results. In the future, we plan to optimise our implementation, particularly the memory footprint of the spatio-temporal workflow, which is currently limited to iteratively processing daily timesteps as the matrices tend to be very large (several gigabytes).

We are also considering improvements to the underlying daylight simulation of our workflows. Progressive photon mapping techniques with visual feedback, for example, would accelerate the simulations and allow a planner to identify (and react to) hotspots early while the results are still being refined.

On a more fundamental level, the light transport simulation should be modified to more efficiently sample adaptively in the spatial *and* temporal domains. The raytracing algorithms currently employed in daylight simulation do not account for the latter, and annual simulations always use large numbers of fixed timesteps, with few actually contributing significantly to the results (i.e. as detectable glare in our analysis).

With this paper, the authors intend to draw attention to the growing problem of glare from BIPV, as well as glass façades in general, and hope that the proposed tools and assessment criteria presented herein will stimulate future research in this field.

Acknowledgments: This was an interdisciplinary effort involving architects, physicists, and computer scientists. We would like to thank the following for their invaluable contributions: digital terrain model of St. Michael's church and its surroundings © GIS Kanton Luzern; our colleague Ran Xu for preparing the digital terrain and church model and exporting it as RADIANCE geometry; our colleague Marek Krehel for obtaining the existing rooftile and PV samples and measuring their BSDFs in our goniophotometer; our colleague Lars Grobe for preparing the data-driven BSDF models for RADIANCE. The application of our workflow to a case study was supported by the city of Lucerne as part of the project *Projektunterstützung Photovoltaik-Anlagen in schützenswerter Umgebung der Stadt Luzern* (#628) submitted by BE Netz AG, Ebikon. This research was supported by the Swiss National Science Foundation as part of the project *ACTIVE INTERFACES - Holistic strategy to simplify standards, assessments and certifications for building integrated photovoltaics* (#153849).

Author Contributions: Stephen Wittkopf initiated this research, supported it with consultations, and wrote the abstract and case study description. Roland Schregle developed the simulation software and workflow scripts, ran the simulations, processed the data, visualised the results, and wrote the relevant sections comprising the bulk of the paper. Christian Renken advised on the proposed criteria and requirements from a practitioner's perspective, wrote the introduction, and provided feedback on the results. All authors reviewed the publication.

Conflicts of Interest: The authors declare no conflict of interest.

Preprints (www.preprints.org) | NOT PEER-REVIEWED | Posted: 21 May 2018 doi:10.20944/preprints201805.0271.v1

Appendix A. Recommende Criteria and Thresholds for Assessing PV Reflection

Table A1 lists criteria and their thresholds recommended by Swissolar [6] which we factored into our simulation and case study. Multiple critical conditions reinforce the likelihood of glare. In addition, we include a conservative irradiance threshold as suggested by Sandia National Laboratories [7] based on experimental data.

Table A1. Recommended PV reflection assessment criteria and thresholds.

Parameter, critical condition	Description	Threshold value	Units
$< \tau_d$	Distance to PV	50 (commercial) 100 (residential)	m
$> \tau_A$	Area of PV	10	m^2
$> \tau_\omega$	Angle subtended by PV at receiver	7.5	° (degrees)
$> \tau_L$	Reflected luminance from PV	50	kcd/m^2
$> \tau_E$	Irradiance from PV at receiver	10 (Sandia Labs) 30 (Swissolar)	W/m^2
$> \tau_t$	Maximum sustained glare duration on any day of the year	30	min
$> \tau_T$	Cumulative glare duration per year	50	hours

Appendix B. Simulation Parameters

Table B2 lists the simulation parameters chosen for PV reflection case study. These coincide with the inputs shown on the left side of our general workflow overview in Figure 4.

Table B2. Simulation parameters for PV reflection case study.

Parameter	Description	Value
DoY	Day of year	[0, 181]
ΔDoY	Day of year increment	7
HoD	Hour of day	[4.5, 20.5]
ΔHoD	Hour of day increment	0.25
N_t	Number of timesteps (sun positions)	1280
Lat, long	Site latitude, longitude	47.038°N, 8.312°E
Merid	Timezone meridian	15°E (CET)
N_p	Number of photons	250M
n_p	Photon lookup bandwith	400 (*rtrace*), 4000 (*rcontrib*)

Preprints (www.preprints.org) | NOT PEER-REVIEWED | Posted: 21 May 2018 doi:10.20944/preprints201805.0271.v1

References

1. Danks, R.; Good, J.; Sinclair, R. Assessing reflected sunlight from building facades: A literature review and proposed criteria. *Building and Environment* **2016**, *103*, 193 – 202. Available online: https://www.sciencedirect.com/science/article/pii/S0360132316301354 (accessed 24.01.2018), doi:10.1016/j.buildenv.2016.04.017.
2. Bundesversammlung der Schweizerischen Eidgenossenschaft. Bundesgesetz über die Raumplanung (Raumplanungsgesetz) RPG; SR 700, 2018. Available online: https://www.admin.ch/opc/de/classified-compilation/19790171/index.html (accessed 6.03.2018).
3. Der Schweizerische Bundesrat. Raumplanungsverordnung RPV; SR700.1, 2016. Available online: https://www.admin.ch/opc/de/classified-compilation/20000959/index.html (accessed 6.03.2018).
4. Reichenbach, A.; Baumann, J.; Hofmann, D.; Nötzli, J.; Vonlanthen, J.; Wyss-Käppeli, B. Vollzugshilfe Lichtemissionen. Technical Report P282-1581, Bundesamt für Umwelt BAFU, 2017. Available online: https://www.bafu.admin.ch/bafu/de/home/themen/elektrosmog/fachinformationen/lichtemissionen--lichtverschmutzung-/konsultation-vollzugshilfe-lichtemissionen.html (accessed 28.03.2018).
5. LAI. Hinweise zur Messung, Beurteilung und Minderung von Lichtimmissionen. Technical report, Bund/Länder-Arbeitsgemeinschaft für Immissionsschutz (LAI), Potsdam, Germany, 2015. Available online: https://www.lai-immissionsschutz.de/documents/hinweise_1503575680.pdf (accessed 26.01.2018).
6. Stickelberger, D.; Moll, C. Leitfaden Solaranlagen. Technical report, Swissolar, Schweizerischer Fachverband für Sonnenenergie, Zürich, 2017. Available online: http://www.swissolar.ch/fileadmin/user_upload/Shop/170707_Leitfaden_RPG_Langfassung.pdf (accessed 26.01.2018).
7. Ho, C.K.; Ghanbari, C.M.; Diver, R.B. Hazard Analyses of Glint and Glare from Concentrating Solar Power Plants. Proceedings of SolarPACES; AIP: Berlin, 2009. Available online: https://www.semanticscholar.org/paper/Hazard-Analyses-of-Glint-and-Glare-from-Solar-Power-Ho-Ghanbari/dcf8c285917f8b46cff00b0be425481c767deb57 (accessed 27.03.2018).
8. Rose, T.; Wollert, A. The dark side of photovoltaic – 3D simulation of glare assessing risk and discomfort. *Environmental Impact Assessment Review* **2015**, *52*, 24 – 30. Available online: http://www.sciencedirect.com/science/article/pii/S0195925514000730 (accessed 23.03.2018), doi:https://doi.org/10.1016/j.eiar.2014.08.005.
9. Sandia National Laboratories. Solar Glare Hazard Analysis Tool (SGHAT), 2017. Available online: https://share.sandia.gov/phlux (accessed 27.03.2018).
10. Sims Industries. GlareGauge – Comprehensive Solar Glare Analysis, 2018. Available online: https://www.forgesolar.com/tools/glaregauge/ (accessed 27.03.2018).
11. Yang, X.; Grobe, L.; Wittkopf, S. Simulation of Reflected Daylight from Building Envelopes. Proceedings Building Simulation 2013; IBPSA: Chambeéry, France, 2013. Available online: http://www.ibpsa.org/proceedings/BS2013/p_1232.pdf (accessed 6.03.2018).
12. Larson, G.W.; Shakespeare, R. *Rendering With Radiance: The Art And Science Of Lighting Visualization*; Booksurge Llc, 2004.
13. Schregle, R. Development and Integration of the RADIANCE Photon Map Extension. Technical report, Lucerne University of Applied Sciences and Arts, 2015. Available online: https://www.researchgate.net/publication/272497518_Development_and_Integration_of_the_RADIANCE_Photon_Map_Extension_v112 (accessed 27.03.2018, doi:10.13140/2.1.3332.9449.
14. Kunz, G. *Kirchen in Luzern*; Baukultur entdecken, Innerschweizer Heimatschutz (IHS), 2009.
15. Kanton Luzern. Geodaten-Portal, 2018. Available online: https://geoportal.lu.ch/geodaten (accessed 16.05.2018).
16. Grobe, L.O.; Wittkopf, S.; Kazanasmaz, Z.T. High-resolution data-driven models of Daylight Redirection Components. *Journal of Façade Design and Engineering* **2017**, *5*, 101–113. Available online: http://ojs-lib.tudelft.nl/index.php/jfde/article/view/1743 (accessed 27.03.2018), doi:10.7480/jfde.2017.2.1743.
17. Ward, G.; Kurt, M.; Bonneel, N. Reducing Anisotropic BSDF Measurement to Common Practice. Proceedings of the Eurographics 2014 Workshop on Material Appearance Modeling: Issues and Acquisition; Eurographics Association: Aire-la-Ville, Switzerland, 2014; MAM '14, pp. 5–8. Available online: http://dl.acm.org/citation.cfm?id=2855560.2855562 (accessed 27.03.2018).

Preprints (www.preprints.org) | NOT PEER-REVIEWED | Posted: 21 May 2018 doi:10.20944/preprints201805.0271.v1

18. Schregle, R.; Grobe, L.; Wittkopf, S. An out-of-core photon mapping approach to daylight coefficients. *Journal of Building Performance Simulation* **2016**, *9*, 620–632. Available online: https://www.tandfonline.com/doi/full/10.1080/19401493.2016.1177116 (accessed 27.03.2018), doi:10.1080/19401493.2016.1177116.
19. Schregle, R. The RADIANCE Photon Map Manual, 2016. doi:10.13140/RG.2.1.4330.8405.
20. Jones, E.; Oliphant, T.; Peterson, P.; et al. SciPy: Open source scientific tools for Python, 2001–. Available online: http://www.scipy.org/ (accessed 14.05.2018).